J. Mietzner, J. Eick, and P. A. Hoeher, "On distributed space-time coding techniques for cooperative wireless networks and their sensitivity to frequency offsets," in *Proc. ITG Workshop on Smart Antennas (WSA 2004)*, Munich, Germany, Mar. 2004, pp. 114–121.

© 2004 IEEE. Personal use of this material is permitted. However, permission to reprint/republish this material for advertising or promotional purposes or for creating new collective works for resale or redistribution to servers or lists, or to reuse any copyrighted component of this work in other works must be obtained from the IEEE.

On Distributed Space-Time Coding Techniques for Cooperative Wireless Networks and their Sensitivity to Frequency Offsets

Jan Mietzner, Jan Eick, and Peter A. Hoeher
Information and Coding Theory Lab, Faculty of Engineering, University of Kiel, Kaiserstrasse 2, D-24143 Kiel, Germany
WWW: www-ict.tf.uni-kiel.de E-mail: {jm,jei,ph}@tf.uni-kiel.de

Abstract— **The application of distributed space-time coding schemes in a simulcast network is considered, and a key challenge is addressed which arises in the downlink: Since the local oscillators employed at the individual transmitting nodes may independently differ from the nominal carrier frequency, frequency offsets will occur between the individual transmission signals. The influence of these frequency offsets on the performance of a specific distributed space-time coding scheme is investigated, and both simulative and analytical results are presented. Appropriate receiver-sided counter measures are considered and possibilities are discussed to estimate the occurring frequency offsets at the receiver.**

Index Terms—**Wireless communications, cooperative networks, distributed space-time coding techniques, frequency offsets.**

I. Introduction

In WIRELESS communications, system performance is often limited by fading, caused by non-constructive interference due to multipath signal propagation. Counter measures, that exploit some sort of *diversity*, significantly improve performance.

In this context, the application of multiple transmit (Tx) and/or multiple receive (Rx) antennas has recently gained much interest [1]. Utilizing the benefits of *spatial* diversity, multiple antenna systems promise large gains over conventional (1x1)-systems with only one Tx and one Rx antenna - especially in rich scattering environments. Spatial diversity results from the fact that the individual transmission paths from the Tx antennas to the Rx antennas are likely to fade independently, i.e., the probability that all paths are degraded at the same time is significantly smaller than the probability that a single transmission path is in a deep fade.

In a multiple antenna system, signal processing is not only performed in the time domain, but also in the spatial domain, i.e., across the individual Tx and Rx antennas. *Space-time codes (STCs)* for multiple antenna systems, such as space-time trellis codes (STTCs) (e.g. [2],[3]) and space-time block codes (STBCs) (e.g. [4],[5]), yield an additional diversity and/or coding gain compared to the (1x1)-system. With STCs, multiple antennas are only required at the transmitter, whereas multiple Rx antennas are optional.

The concept of multiple antennas may be transferred to *cooperative* wireless networks, in which multiple (single-antenna) nodes cooperate in order to realize a joint transmission strategy. Just as in a multiple-antenna system, the nodes may exploit spatial diversity by sharing their antennas in the context of a *distributed* STC scheme ('cooperative diversity'). Examples for cooperative wireless networks include simulcast networks (e.g. [6],[7]) and relay-assisted networks (e.g. [8]-[10]).

Simulcast networks are, for example, employed for broadcasting or for paging applications, i.e., either when many mobile users shall be served simultaneously or when the position of a single desired user is unknown. Conventionally, several serving nodes simultaneously transmit the same signal using the same carrier frequency. In cellular networks, simulcasting may be used in areas that are served by multiple base stations in order to reduce the probability of shadowing. However, conventional simulcasting does not yield a diversity gain [6].

In a relay-assisted network, the transmitted signal of a certain source node, e.g., a mobile station, is received by several relay nodes, which then forward the signal to a certain destination node. Relaying may either be performed by fixed stations or by other mobile stations, as in [8]. Application examples include cellular systems, sensor networks, and ad-hoc networks.

Distributed STC techniques are suitable both for simulcast networks and for relay-assisted networks. In particular, a relay-assisted network may be viewed as a special type of simulcast network, if only a few transmission errors occur between the source node and the relay nodes and if the individual relays simultaneously transmit on the same carrier frequency.

Within the scope of this paper, the focus is on simulcast networks. A key challenge shall be addressed that arises in the *downlink*: The local oscillators (LOs) employed at the individual transmitting nodes may independently differ from the nominal carrier frequency f_c, because a coupling between the LOs cannot be presumed. Due to this, frequency offsets with respect to f_c will occur between the individual transmission signals.

The paper is organized as follows: Section II introduces the topology of the simulcast network as well as the class of STC schemes considered throughout this paper. Focus is on the well-known Alamouti scheme for two Tx antennas [11],[12].

In Section III, it is shown that the orthogonality of the Alamouti scheme is lost in the presence of frequency offsets (see also [13]), which causes severe performance degradations if no counter measures are applied. Three different receiver concepts are considered and their performance is determined on the basis of simulative and analytical results:

(i) Conventional Alamouti detection using the hermitian conjugate of the equivalent orthogonal channel matrix.
(ii) Zero-forcing detection using the inverse of the equivalent orthogonal channel matrix.
(iii) Maximum-likelihood detection.

In this context, the following scenarios are addressed:

(a) The occurring frequency offsets are perfectly known at the receiver.
(b) Non-perfect estimates of the frequency offsets are available at the receiver.

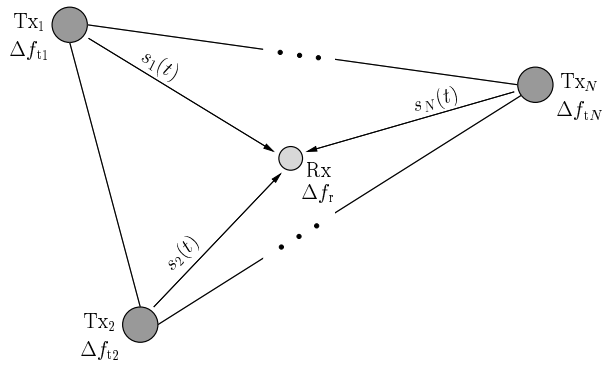

Fig. 1. Simulcast network with N transmitting nodes and one receiving node.

(c) The frequency offsets are completely unknown at the receiver.

Concerning scenario (b), two possible frequency-offset estimation techniques are discussed in Section IV: A training-based estimation method and a blind estimation method. Specifically, it is illustrated that frequency-offset estimation in cooperative wireless networks is more difficult than frequency-offset estimation in systems with only a single transmitting node. Concluding remarks are given in Section V.

II. Simulcast Network Topology and Class of Distributed Space-Time Coding Schemes

An example for a simulcast network with N transmitting nodes and one receiving node is given in Fig. 1. It is assumed that all nodes employ a single antenna. If no shadowing occurs, a diversity degree of N may be achieved by means of an appropriate distributed STC scheme for N Tx antennas. For instance, an orthogonal STBC [4],[5] may be employed. On the one hand, orthogonal STBCs achieve full diversity in terms of the number of transmitting nodes. On the other hand, they have another property that is desirable for the application under consideration [9]: If *any* subset of $n < N$ transmitting nodes is completely obstructed due to shadowing, orthogonal STBCs still grant a diversity degree of $(N-n)$. A drawback of these STC schemes is, however, that for $N > 2$ no orthogonal STBC exists with a temporal rate of one [14]. For $N = 2$, the well-known Alamouti scheme [11], which also belongs to the class of orthogonal STBCs, provides a temporal rate of one; therefore the focus shall be on this case here. Even if there are more than two transmitting nodes available, it may still be useful to employ the Alamouti scheme – in conjunction with a *selection diversity* scheme [15] choosing those two nodes that are associated with the best transmission paths toward the receiving node, e.g., in terms of signal-to-noise ratio (SNR).

In the following, it is assumed that the ν-th transmitting node (Tx_ν) of the simulcast network has a frequency offset $\Delta f_{\mathrm{t}\nu}$, and the receiving node (Rx) has a frequency offset Δf_{r} (cf. Fig. 1). Then, the overall frequency offset associated with the transmitted signal $s_\nu(t)$ is given by [13]

$$\Delta f_\nu \;=\; \Delta f_{\mathrm{t}\nu} - \Delta f_{\mathrm{r}}. \tag{1}$$

Throughout the paper, the normalized frequency offset

$$\zeta_\nu \;\doteq\; \Delta f_\nu \, T \tag{2}$$

is of interest, where T denotes the symbol duration. It is assumed here that $|\zeta_\nu| \leq 0.04$ for all ν, which appears to be relevant for most practical wireless communication systems.

III. Influence of the Frequency Offsets

In this section, the influence of the frequency offsets introduced by the individual transmitting nodes shall be investigated on the basis of a distributed Alamouti scheme ($N = 2$). To start with, the Alamouti scheme is briefly reviewed. Throughout this paper, the equivalent complex baseband representation is used.

A. Review of the Alamouti Scheme

The Alamouti scheme [11] was designed for quasi-static frequency-flat fading channels. In the Alamouti scheme, M-ary data symbols are processed as pairs $[\,x[k], x[k+1]\,]$ and transmitted over two antennas according to

$$\mathbf{A}[k] \doteq \underbrace{\begin{bmatrix} x[k] & -x^*[k+1] \\ x[k+1] & x^*[k] \end{bmatrix}}_{\begin{matrix}\uparrow \\ \text{Antenna 1}\end{matrix} \quad \begin{matrix}\uparrow \\ \text{Antenna 2}\end{matrix}} \begin{matrix}\longleftarrow \text{ Time index } k \\ \longleftarrow \text{ Time index } k+1\end{matrix} \tag{3}$$

where $(.)^*$ denotes complex conjugation[1]. The Alamouti matrix $\mathbf{A}[k]$ is orthogonal and

$$\mathbf{A}^{\mathrm{H}}[k]\,\mathbf{A}[k] \;=\; \left(|x[k]|^2 + |x[k+1]|^2\right)\,\mathbf{I}_2\,, \tag{4}$$

where $\mathbf{A}^{\mathrm{H}}[k]$ is the hermitian conjugate of $\mathbf{A}[k]$, and $\mathbf{I}_2$ is the identity matrix of size (2×2).

Given a quasi-static frequency-flat fading channel, each transmission path from Tx antenna ν ($\nu = 1, 2$) to the Rx antenna can be modeled by means of a single complex-valued channel coefficient h_ν, which is constant over the duration of an entire data block. Taking into account the space-time mapping according to the Alamouti matrix $\mathbf{A}[k]$, the received symbols $y[k]$ and $y[k+1]$ are given by the following matrix equation [16, Ch. 7.3.2]:

$$\underbrace{\begin{bmatrix} y[k] \\ y^*[k+1] \end{bmatrix}}_{\mathbf{y}[k]} = \tag{5}$$

$$c \cdot \underbrace{\begin{bmatrix} h_1 & -h_2 \\ h_2^* & h_1^* \end{bmatrix}}_{\mathbf{H}_{\mathrm{eq}}} \underbrace{\begin{bmatrix} x[k] \\ x^*[k+1] \end{bmatrix}}_{\mathbf{x}[k]} + \underbrace{\begin{bmatrix} n[k] \\ n^*[k+1] \end{bmatrix}}_{\mathbf{n}[k]},$$

where $c > 0$ is a real-valued normalization factor[2] and $n[k]$ and $n[k+1]$ denote samples of a complex additive white Gaussian

[1] In this paper, the transposed of the original matrix [11] is used.

[2] For a fair comparison with a (1x1)-system, the overall transmitted power should be normalized with respect to the number of Tx antennas used, i.e., c should be chosen as $c \doteq 1/\sqrt{2}$.

noise (AWGN) process with zero mean and variance σ_n^2, taken at time index k and $k+1$, respectively. The equivalent (2×2) channel matrix $\mathbf{H}_{eq}$ is orthogonal, which is due to the orthogonality of the Alamouti matrix $\mathbf{A}[k]$. This property enables maximum-ratio combining (MRC) at the receiver by means of the following simple matrix multiplication, provided that the channel coefficients are perfectly known:

$$\mathbf{z}[k] \doteq \mathbf{H}_{eq}^{H}\,\mathbf{y}[k] = c\,\mathbf{H}_{eq}^{H}\mathbf{H}_{eq}\,\mathbf{x}[k] + \mathbf{H}_{eq}^{H}\,\mathbf{n}[k], \quad \text{where}$$

$$\mathbf{H}_{eq}^{H}\mathbf{H}_{eq} = \underbrace{\left(|h_1|^2+|h_2|^2\right)}_{\doteq\,\theta}\mathbf{I}_2 \doteq \mathbf{\Theta} \tag{6}$$

and $\mathbf{z}[k] \doteq [\,z[k], z^*[k+1]\,]^T$ denotes the soft estimate of $\mathbf{x}[k]$. As can be seen, the orthogonality of $\mathbf{H}_{eq}$ leads to a decoupling of $x[k]$ and $x[k+1]$ in terms of *independent* soft estimates $z[k]$ and $z[k+1]$. Due to the diagonal structure of $\mathbf{\Theta}$, the desired symbols are always combined in a constructive way, because they are multiplied by a sum of absolute terms. The noise, however, is combined incoherently (matrix $\mathbf{H}_{eq}^{H}$), which leads to a diversity gain over the (1x1)-system.

B. Orthogonality Loss Due to Frequency Offsets

The orthogonality of the Alamouti scheme is lost in the presence of frequency offsets ζ_ν $(\nu = 1, 2)$ [13]. This will cause more or less severe performance degradations, depending on whether the receiver is able to exploit knowledge about the frequency offsets.

In the following, it is assumed that the receiver has perfect knowledge of the channel coefficients h_1 and h_2 at the beginning of each data block, so as to isolate the effects of the frequency offsets. Time-varying variables are in the sequel denoted by $\overline{(.)}$. For the time being, a single data block shall be considered.

Due to the frequency offsets, the channel coefficients are associated with a time-varying phase term, according to

$$\overline{h}_\nu[k] \doteq h_\nu \cdot e^{j2\pi\zeta_\nu k}, \qquad \nu = 1, 2. \tag{7}$$

This leads to a modified channel matrix, which is now time-varying:

$$\overline{\mathbf{H}}_{eq}[k] = \begin{bmatrix} \overline{h}_1[k] & -\overline{h}_2[k] \\ \overline{h}_2^*[k+1] & \overline{h}_1^*[k+1] \end{bmatrix}. \tag{8}$$

Three different scenarios shall be considered here, regarding knowledge of the frequency offsets ζ_ν at the receiver (further details may be found in [13]):

(a) The frequency offsets are *perfectly* known. Then, the receiver may use the above matrix $\overline{\mathbf{H}}_{eq}[k]$, in order to perform symbol detection according to (6). The product matrix
$$\overline{\mathbf{H}}_{eq}^{H}[k]\,\overline{\mathbf{H}}_{eq}[k] \doteq \overline{\mathbf{\Theta}}[k]$$
does not exactly yield a diagonal matrix, as opposed to the matrix $\mathbf{\Theta}$ in (6). However, this orthogonality loss tends to be rather small for practical values of ζ_1 and ζ_2, i.e., $\overline{\mathbf{\Theta}}[k]$ is close to a diagonal matrix for all k.

(b) *Non-perfect* estimates $\hat{\zeta}_\nu$ of the frequency offsets are available at the receiver, where
$$\hat{\zeta}_\nu \doteq \zeta_\nu + \epsilon_\nu.$$
Then, the receiver may use the matrix
$$\overline{\mathbf{H}}_{eq,\epsilon}[k] = \begin{bmatrix} h_1 \cdot e^{j2\pi\hat{\zeta}_1 k} & -h_2 \cdot e^{j2\pi\hat{\zeta}_2 k} \\ h_2^* \cdot e^{-j2\pi\hat{\zeta}_2(k+1)} & h_1^* \cdot e^{-j2\pi\hat{\zeta}_1(k+1)} \end{bmatrix}$$
for symbol detection. Depending on the quality of the estimates $\hat{\zeta}_\nu$, the orthogonality loss may be more or less severe. The desired symbols are not necessarily combined in a constructive way anymore, and the non-zero secondary diagonal elements of the product matrix
$$\overline{\mathbf{H}}_{eq,\epsilon}^{H}[k]\,\overline{\mathbf{H}}_{eq}[k] \doteq \overline{\mathbf{\Theta}}_\epsilon[k]$$
may cause significant interference between the data symbols $x[k]$ and $x[k+1]$.

(c) The frequency offsets are completely *unknown*. Then, the receiver will still use matrix $\mathbf{H}_{eq}$ for symbol detection. Depending on k, the diagonal elements of the product matrix
$$\mathbf{H}_{eq}^{H}\,\overline{\mathbf{H}}_{eq}[k] \doteq \overline{\mathbf{\Upsilon}}[k]$$
can be close to zero whereas the secondary diagonal elements can assume large values. This will cause severe performance degradations.

In the following, two enhanced receiver concepts shall be discussed, namely zero-forcing (ZF) detection (e.g. [17]), and maximum-likelihood (ML) detection, where the focus is on the above scenarios (a) and (b).

C. Zero-Forcing (ZF) Detection

Instead of using the hermitian conjugate of the matrix $\overline{\mathbf{H}}_{eq}[k]$ in the case of perfect knowledge of the frequency offsets, as done in the conventional Alamouti detection scheme, the *inverse* matrix $\overline{\mathbf{H}}_{eq}^{-1}[k]$ is used for symbol detection. This yields the soft estimate

$$\mathbf{z}_{ZF}[k] \doteq \overline{\mathbf{H}}_{eq}^{-1}[k]\,\mathbf{y}[k] = c\,\mathbf{x}[k] + \overline{\mathbf{H}}_{eq}^{-1}[k]\,\mathbf{n}[k]. \tag{9}$$

The determinant of $\overline{\mathbf{H}}_{eq}[k]$ is given by

$$\det\left(\overline{\mathbf{H}}_{eq}[k]\right) = |h_1|^2\,e^{-j2\pi\zeta_1} + |h_2|^2\,e^{-j2\pi\zeta_2}. \tag{10}$$

Since it is assumed that $|\zeta_1|, |\zeta_2| \ll 1$, the condition of $\overline{\mathbf{H}}_{eq}[k]$ is virtually determined solely by the magnitude of the channel coefficients. If the frequency offsets ζ_ν are zero, ZF detection is equivalent to conventional Alamouti detection, where

$$\overline{\mathbf{H}}_{eq}^{-1}[k] = \frac{1}{\theta}\,\overline{\mathbf{H}}_{eq}^{H}[k].$$

Eq. (9) may be rewritten by using the Moore-Penrose pseudoinverse [17] of $\overline{\mathbf{H}}_{eq}[k]$:

$$\overline{\mathbf{H}}_{eq}^{+}[k] \doteq \left(\overline{\mathbf{H}}_{eq}^{H}[k]\,\overline{\mathbf{H}}_{eq}[k]\right)^{-1}\overline{\mathbf{H}}_{eq}^{H}[k].$$

Therefore, ZF detection may be interpreted as an add-on to conventional Alamouti detection:

$$\mathbf{z}_{\mathrm{ZF}}[k] \;=\; \overline{\mathbf{H}}_{\mathrm{eq}}^{+}[k]\,\mathbf{y}[k] \;=\; \left(\overline{\mathbf{H}}_{\mathrm{eq}}^{\mathrm{H}}[k]\,\overline{\mathbf{H}}_{\mathrm{eq}}[k]\right)^{-1}\overline{\mathbf{H}}_{\mathrm{eq}}^{\mathrm{H}}[k]\;\mathbf{y}[k]$$
$$=\; \left(\overline{\mathbf{H}}_{\mathrm{eq}}^{\mathrm{H}}[k]\,\overline{\mathbf{H}}_{\mathrm{eq}}[k]\right)^{-1}\mathbf{z}[k]\,. \qquad (11)$$

As can be seen in (9), ZF detection completely removes interference (see term $c\,\mathbf{x}[k]$). However, it is well known that ZF detection may also lead to noise enhancement, depending on the condition of $\overline{\mathbf{H}}_{\mathrm{eq}}[k]$. An improvement of ZF detection is referred to as minimum-mean-square-error (MMSE) detection (e.g. [17]), which is in this case given by

$$\mathbf{z}_{\mathrm{MMSE}}[k] \;=\; \left(\overline{\mathbf{H}}_{\mathrm{eq}}^{\mathrm{H}}[k]\,\overline{\mathbf{H}}_{\mathrm{eq}}[k] + \sigma_{\mathrm{n}}^2\,\mathbf{I}_2\right)^{-1}\overline{\mathbf{H}}_{\mathrm{eq}}^{\mathrm{H}}[k]\;\mathbf{y}[k]\,. \qquad (12)$$

MMSE detection yields the minimum overall distortion due to residual interference and noise.

Simulation results (see Section III-G) show that the performance of ZF detection is already virtually the same as that of ML detection (see following section). Therefore, MMSE detection shall not be considered in the sequel.

Applying ZF detection in the case of non-perfect frequency-offset estimates at the receiver means that, as opposed to (9), the interference is not completely removed:

$$\mathbf{z}_{\mathrm{ZF}}[k] \;=\; \overline{\mathbf{H}}_{\mathrm{eq},\epsilon}^{-1}[k]\,\mathbf{y}[k] \;=\; c\,\overline{\mathbf{\Theta}}_{\mathrm{ZF},\epsilon}[k]\,\mathbf{x}[k] \;+\; \overline{\mathbf{H}}_{\mathrm{eq},\epsilon}^{-1}[k]\,\mathbf{n}[k]$$

(cf. (5)), where

$$\overline{\mathbf{\Theta}}_{\mathrm{ZF},\epsilon}[k] \;\doteq\; \overline{\mathbf{H}}_{\mathrm{eq},\epsilon}^{-1}[k]\,\overline{\mathbf{H}}_{\mathrm{eq}}[k] \;\neq\; \mathbf{I}_2\,.$$

D. Maximum-Likelihood (ML) Detection

In the case of perfect knowledge of the frequency offsets at the receiver, the ML estimate of $\mathbf{x}[k]$ is given by

$$\hat{\mathbf{x}}_{\mathrm{ML}}[k] \;=\; \underset{\tilde{\mathbf{x}}[k]}{\mathrm{argmin}}\,\left|\,\mathbf{y}[k] \;-\; c\,\overline{\mathbf{H}}_{\mathrm{eq}}[k]\,\tilde{\mathbf{x}}[k]\,\right|^2, \qquad (13)$$

where $\tilde{\mathbf{x}}[k]$ denotes a hypothesis for the M-ary data symbol vector $\mathbf{x}[k]$. For each ML estimate $\hat{\mathbf{x}}_{\mathrm{ML}}[k]$, M^2 different metrics have to be computed, corresponding to the M^2 possible hypotheses $\tilde{\mathbf{x}}[k]$. As opposed to conventional Alamouti detection or ZF detection, ML detection yields hard estimates, which are therefore denoted by a vector $\hat{\mathbf{x}}_{\mathrm{ML}}[k]$ rather than by a vector $\mathbf{z}_{\mathrm{ML}}[k]$. If the frequency offsets ζ_ν are zero, the ML estimate $\hat{\mathbf{x}}_{\mathrm{ML}}[k]$ is equivalent to a hard decision on the corresponding soft estimate obtained by conventional Alamouti detection or ZF detection. Given non-perfect frequency-offset estimates, the matrix $\overline{\mathbf{H}}_{\mathrm{eq},\epsilon}[k]$ is used to calculate the metric (13) instead of $\overline{\mathbf{H}}_{\mathrm{eq}}[k]$, which leads to a systematic error.

E. Receiver Complexities

The receiver complexities for conventional Alamouti detection and for ZF detection do not depend on the cardinality M of the symbol alphabet. For conventional Alamouti detection, about 20 floating point operations (flops) are required for each soft estimate $\mathbf{z}[k]$, and for ZF detection about 30 flops (including matrix inversion). In contrast to this, the number of flops required for an ML estimate $\hat{\mathbf{x}}_{\mathrm{ML}}[k]$ grows with M^2. The approximate receiver complexities resulting for different values of M are stated in Table I. As can be seen, the complexity of ML detection is well above the one for conventional Alamouti detection or ZF detection, already for $M = 4$. In the following, ML detection shall be used as a benchmark concerning system performance. For a practical implementation, however, it seems to be less attractive, due to the good results obtained with ZF detection (cf. Section III-G).

TABLE I
RECEIVER COMPLEXITIES PER ESTIMATE FOR DIFFERENT CARDINALITIES OF THE SYMBOL ALPHABET

Cardinality M	Example	Conv. Alamouti	ZF	ML
2	BPSK	20	30	110
4	QPSK	20	30	430
8	8-PSK	20	30	1700
16	16-QAM	20	30	7000
64	64-QAM	20	30	110000

F. Bit Error Probability in Case of Non-Ideal Local Oscillators

In [13], analytical expressions for the bit error probability (BEP) are derived, for the example of QPSK ($M = 4$) and a quasi-static frequency-flat fading channel. These BEP expressions apply for conventional Alamouti detection as well as for ZF detection.

Let b_{1k} and b_{2k} denote the first and the second bit mapped on the quaternary data symbol $x[k]$, $[b_{1k}\,b_{2k}] \mapsto x[k]$, and let $z[k]$ denote the corresponding soft estimate, either obtained by conventional Alamouti detection or by ZF detection. Gray mapping of the bits is assumed according to

$$[00] \mapsto \exp[\mathrm{j}\,\pi/4] \qquad [01] \mapsto \exp[\mathrm{j}\,3\pi/4]$$
$$[11] \mapsto \exp[\mathrm{j}\,5\pi/4] \qquad [10] \mapsto \exp[\mathrm{j}\,7\pi/4].$$

Let $d_{\mathrm{Re}}[k] \doteq \mathrm{Re}\{z[k]\}$ and $d_{\mathrm{Im}}[k] \doteq \mathrm{Im}\{z[k]\}$ denote the real and the imaginary part of $z[k]$ for $E_s/N_0 \to \infty$, respectively (E_s denotes the average energy per data symbol and N_0 the single-sided noise spectral density). Since $d_{\mathrm{Im}}[k]$ is the distance between $z[k]$ and the decision threshold for bit b_{1k}, the BEP for b_{1k} is given by [18, Ch. 5.2]

$$P_{\mathrm{b1}}[k] \;=\; \mathrm{Q}\left(\sqrt{2\,\frac{d_{\mathrm{Im}}^2[k]}{\theta}\,\frac{E_s}{N_0}}\right), \qquad (14)$$

if the imaginary parts of $x[k]$ and $z[k]$ have equal signs, otherwise by

$$P_{\mathrm{b1}}[k] \;=\; \bar{\mathrm{Q}}\left(\sqrt{2\,\frac{d_{\mathrm{Im}}^2[k]}{\theta}\,\frac{E_s}{N_0}}\right), \qquad (15)$$

where $\bar{\mathrm{Q}}(t) \doteq 1 - \mathrm{Q}(t)$. Along the same lines, the bit error probability $P_{\mathrm{b2}}[k]$ for the second bit may be calculated,

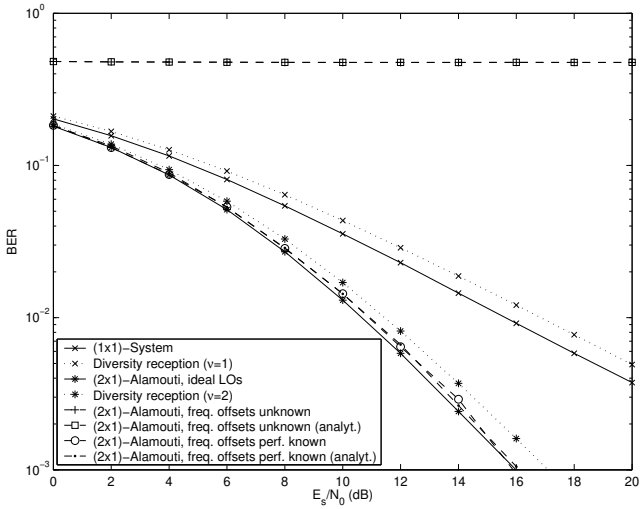

Fig. 2. Performance results for conventional Alamouti detection, given (a) ideal local oscillators (LOs), (b) non-ideal LOs, frequency offsets completely unknown at the receiver, and (c) perfect knowledge of the frequency offsets.

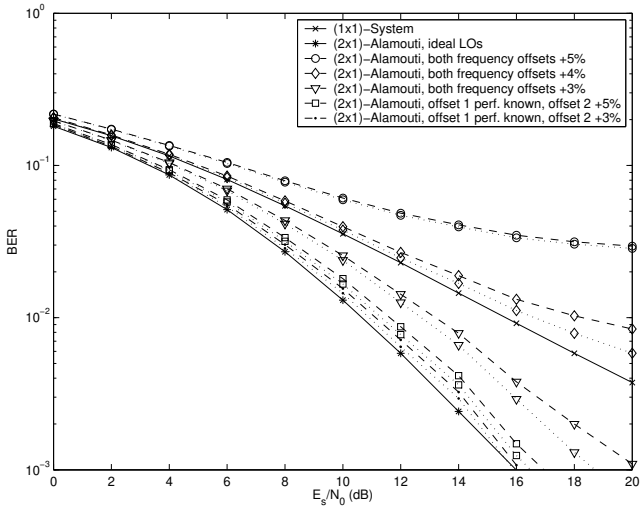

Fig. 3. Comparison between conventional Alamouti detection (dashed lines) and ML detection (dotted lines) for the case of non-perfect estimates of the frequency offsets at the receiver. The performance of ZF detection is virtually the same as that of ML detection in all cases.

using $d^2_{\mathrm{Re}}[k]$. Analytical expressions for the distances $d_{\mathrm{Re}}[k]$ and $d_{\mathrm{Im}}[k]$ as a function of the channel coefficients and the frequency offsets are developed in [13]. It is straightforward to extend this to the case of ZF detection.

The expectation of the bit error probability $P_{\mathrm{b}i}[k]$ $(i = 1, 2)$ with respect to the channel coefficients is given by

$$\bar{P}_{\mathrm{b}i}[k] \;=\; \int p_h(\mathbf{h})\; P_{\mathrm{b}i}[k]\; \mathrm{d}\mathbf{h}\,, \tag{16}$$

where $p_h(\mathbf{h})$ denotes the joint pdf of the channel coefficients. The integral is over all possible realizations of $\mathbf{h}$.The overall average bit error probability, given blocks of L_{B} QPSK symbols, results as

$$\bar{P}_{\mathrm{b}} \;=\; \frac{1}{2L_{\mathrm{B}}} \sum_{k=0}^{L_{\mathrm{B}}-1} \bar{P}_{\mathrm{b}1}[k] + \bar{P}_{\mathrm{b}2}[k]\,. \tag{17}$$

G. Simulation Results

For perfect and for non-perfect knowledge of the frequency offsets at the receiver, the performance loss shall be illustrated in the following, which results for the distributed Alamouti scheme, given the different receiver concepts discussed earlier.

For the simulations, it was assumed that there is a significant line-of-sight signal component between either transmitting node and the receiving node. In this context, a quasi-static frequency-flat Rician fading channel model with a Rice factor of $K = 0$ dB was used for both transmission paths. The simulation results were obtained by means of Monte-Carlo simulations. Each block contained $L_{\mathrm{B}} = 100$ QPSK symbols ($M = 4$, Gray mapping used). Channel coding has not been applied. An outer channel code may, however, be added to further improve performance.

To start with, frequency offsets $\zeta_1 = +0.03$ and $\zeta_2 = -0.012$ were considered. At the receiver, the channel coefficients were perfectly known at the beginning of each block, i.e., the observed performance degradations are solely due to the time-varying phases caused by the frequency offsets. The transmit power was always normalized with respect to the number of transmitting nodes, in order to provide a fair comparison between the distributed Alamouti scheme and the case when there is only a single transmitting node ('(1x1)-system').

Fig. 2 presents performance results for conventional Alamouti detection, in terms of bit error rate (BER) vs. E_s/N_0 in dB. Moreover, analytical curves (dotted lines) are included [18, Ch. 14.4] for *diversity reception* of uncoded QPSK over ν statistically independent Rayleigh fading channels ($\nu = 1, 2$) with identical average signal-to-noise ratios (SNRs) of $(E_s/N_0)/\nu$. As can be seen, the BER performance of the (1x1)-system is slightly better than the analytical curve for $\nu = 1$, which is due to the line-of-sight signal component. Likewise, given ideal LOs (i.e., frequency offsets equal to zero), the BER performance of the Alamouti scheme is slightly better than the analytical curve for $\nu = 2$. The dashed lines represent the two extreme cases of unknown and perfectly known frequency offsets at the receiver. The corresponding analytical curves obtained on the basis of Section III-F are as well included. The average bit error probability according to (16) and (17) was computed by averaging over 10.000 realizations of the channel coefficients. As can be seen, simulative and analytical curves are in good accordance. For perfect knowledge of the frequency offsets at the receiver, the BER performance is very close to the case of ideal LOs, since the loss of orthogonality is rather small (cf. Section III-B). When the frequency offsets are unknown, however, a huge average BER of about 0.5 results for all values of E_s/N_0.

A comparison between conventional Alamouti detection (dashed lines) and ML detection (dotted lines) is presented in Fig. 3, for the case of non-perfect estimates of the frequency offsets at the receiver. The performance of ZF detection is virtually the same as that of ML detection in all cases. Therefore, the simulation results for ZF detection are omitted in the plot.

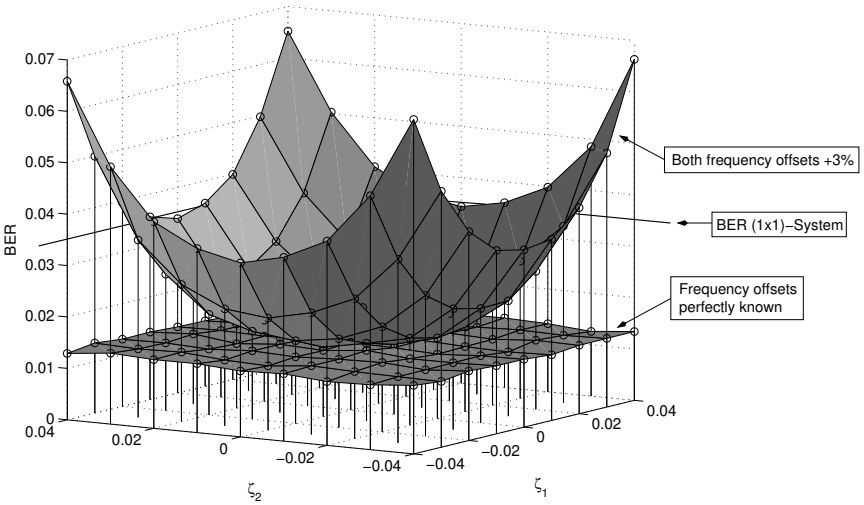

Fig. 4. Performance results for ML detection ($E_s/N_0 = 10$ dB), given frequency offsets $|\zeta_1|, |\zeta_2| < 0.04$ and (a) perfect knowledge of the frequency offsets at the receiver, (b) non-perfect frequency-offset estimates at the receiver (both frequency offsets estimated with an error of +3%).

As can be seen, a performance loss of less than 1 dB occurs at a BER of 10^{-3}, with respect to the case of ideal LOs, if one frequency offset is perfectly known and the other one is estimated with an error of 5% or better. ML/ZF detection yields only small improvements over conventional Alamouti detection. However, as will be shown in Section IV, it is more realistic to assume that a certain estimation error occurs for both frequency offsets. In this case, the performance loss is more severe. Only if both frequency offsets are estimated with an error of 3% or better, the system performance is superior to that of the (1x1)-system. In this case, ML/ZF detection yields a 1.5 dB gain over conventional Alamouti detection, at a BER of 10^{-3}.

So far, only a single pair ζ_1,ζ_2 of frequency offsets has been considered. Fig. 4 shows simulation results for the BER performance in the case of ML detection, given frequency offsets $|\zeta_1|, |\zeta_2| \leq 0.04$ ($E_s/N_0 = 10$ dB). The case of perfectly known frequency offsets at the receiver is displayed as well as the case, where both frequency offsets are estimated with an error of +3%. As a reference, the BER of the (1x1)-system is also included. As can be seen, for large frequency offsets the diversity gain over the (1x1)-system is lost.

Within the scope of this paper, only receiver-sided concepts to compensate for the frequency offsets have been discussed. Alternatively, a closed-loop scheme may be employed, where the receiving node feeds back the frequency-offset estimates to the transmitting nodes via a dedicated channel. The frequency offsets may then be corrected directly at the transmitters. In this case, significantly less accurate frequency-offset estimates are required. For example, given a frequency offset of $\zeta = 0.04$ and an estimation error of 3%, the frequency offset may theoretically be reduced to $|\zeta'| = 0.0012$, which virtually leads to the same BER performance as in the case of ideal LOs.

IV. Frequency-Offset Estimation

In this section, a training-based and a blind frequency-offset estimation technique are investigated. Specifically, it is illustrated that frequency-offset estimation in cooperative wireless networks is more difficult than in systems with a single transmitting node.

A. Training-Based Estimation Method

If the frequency offsets are zero, (5) may be rewritten as

$$\mathbf{y}'[k] \;=\; c\,\mathbf{A}[k]\,\mathbf{h} \;+\; \mathbf{n}'[k], \tag{18}$$

where

$$\begin{aligned} \mathbf{y}'[k] &\doteq [\,y[k], y[k+1]\,]^{\mathrm{T}}, \\ \mathbf{n}'[k] &\doteq [\,n[k], n[k+1]\,]^{\mathrm{T}}, \\ \mathbf{h} &\doteq [\,h_1, h_2\,]^{\mathrm{T}}, \end{aligned}$$

and $\mathbf{A}[k]$ according to (3). Obtaining an estimate for $\mathbf{h}$, given known training symbols, is dual to obtaining an estimate for $\mathbf{x}[k]$, given known channel coefficients (cf. (6)):

$$\hat{\mathbf{h}}[k] \;\doteq\; c\,\mathbf{A}^{\mathrm{H}}[k]\,\mathbf{y}'[k] \;=\; \mathbf{h} \;+\; c\,\mathbf{A}^{\mathrm{H}}[k]\,\mathbf{n}'[k]\,, \tag{19}$$

assuming $c = 1/\sqrt{2}$ and $|x[\,.\,]|^2 = 1$ (cf. (4)).

In the case of non-zero frequency offsets, however, (18) holds only approximately:

$$\mathbf{y}'[k] \;\approx\; c\,\mathbf{A}[k]\,\overline{\mathbf{h}}[k] \;+\; \mathbf{n}'[k]\,, \tag{20}$$

where

$$\overline{\mathbf{h}}[k] \;\doteq\; [\,\overline{h}_1[k], \overline{h}_2[k+1]\,]^{\mathrm{T}},$$

(cf. (7)). The error vector $\mathbf{e}[k] \doteq \mathbf{y}'[k] - (c\,\mathbf{A}[k]\,\overline{\mathbf{h}}[k] \;+\; \mathbf{n}'[k])$ is given by

$$\mathbf{e}[k] \;=\; c \begin{bmatrix} h_2\,x^*[k+1]\left(\mathrm{e}^{\mathrm{j}2\pi\zeta_2 k} - \mathrm{e}^{\mathrm{j}2\pi\zeta_2(k+1)}\right) \\ h_1\,x[k+1]\left(\mathrm{e}^{\mathrm{j}2\pi\zeta_1 k} - \mathrm{e}^{\mathrm{j}2\pi\zeta_1(k+1)}\right) \end{bmatrix}. \tag{21}$$

Therefore, the corresponding estimate for $\overline{\mathbf{h}}[k]$,

$$\hat{\overline{\mathbf{h}}}[k] \;=\; \overline{\mathbf{h}}[k] \;+\; c\,\mathbf{A}^{\mathrm{H}}[k]\,(\mathbf{n}'[k] \;+\; \mathbf{e}[k])\,, \tag{22}$$

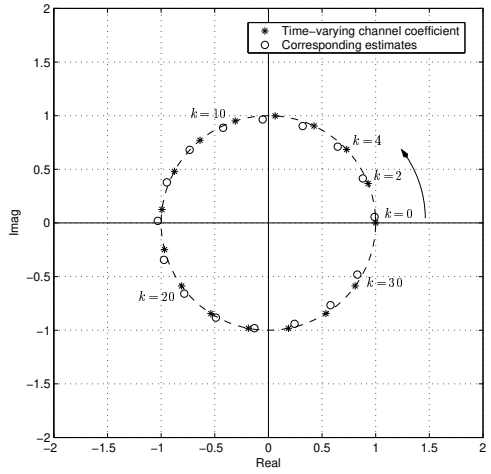

Fig. 5. Time-varying channel coeffi cient $\overline{h}_1[k]$ and the corresponding estimate depicted within the complex plane, for $E_s/N_0 \to \infty$ and different values of k.

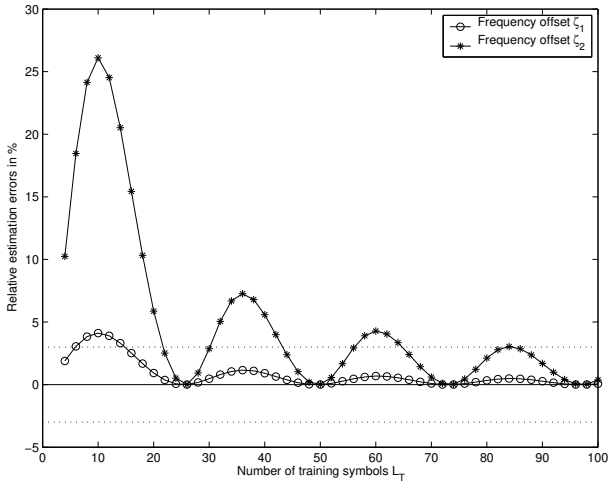

Fig. 6. Relative estimation errors as a function of the number of training symbols, L_{T}, concerning estimation of ζ_1 and ζ_2 for $E_s/N_0 \to \infty$.

is erroneous even if the noise is zero. This fact is illustrated in Fig. 5, where the first channel coefficient $\overline{h}_1[k]$ and the corresponding estimate $\hat{\overline{h}}_1[k]$ is depicted within the complex plane, for $E_s/N_0 \to \infty$ and different values of k. The frequency offsets were again chosen as $\zeta_1 = +0.03$ and $\zeta_2 = -0.012$. The magnitude of $\overline{h}_1[k]$ was set to one and all training symbols $x[\,.\,]$ were $+1$.

In the sequel, explicit estimates for the frequency offsets ζ_1 and ζ_2 shall be calculated. Typically, frequency offsets may be considered time-invariant. Therefore, it is sufficient to perform a one-shot estimation using a single block of L_{T} training symbols (L_{T} even). Essentially, estimates for the frequency offsets may be obtained on basis of several subsequent estimated vectors $\hat{\overline{\mathbf{h}}}[k]$ by averaging over the associated phase differences:

$$\hat{\zeta}_1(L_{\mathrm{T}}) \;=\; \frac{1}{\mathrm{j}\,4\pi\,S} \sum_{\substack{k=2 \\ k\ \mathrm{even}}}^{L_{\mathrm{T}}-2} \arg\left\{ \frac{\hat{\overline{h}}_1[k]}{\hat{\overline{h}}_1[k-2]} \right\},$$

$$\hat{\zeta}_2(L_{\mathrm{T}}) \;=\; \frac{1}{\mathrm{j}\,4\pi\,S} \sum_{\substack{k=3 \\ k\ \mathrm{odd}}}^{L_{\mathrm{T}}-1} \arg\left\{ \frac{\hat{\overline{h}}_2[k]}{\hat{\overline{h}}_2[k-2]} \right\},$$

where $S \doteq L_{\mathrm{T}}/2 - 1$. In Fig. 6 and Fig. 7, examples are given for the relative estimation errors

$$e_\nu(L_{\mathrm{T}}) \doteq \frac{\hat{\zeta}_\nu(L_{\mathrm{T}}) - \zeta_\nu}{\zeta_\nu}, \qquad \nu = 1, 2$$

as a function of L_{T}, for $E_s/N_0 \to \infty$ and $E_s/N_0 = 20$ dB, respectively (frequency offsets ζ_1 and ζ_2 as above, magnitudes of $\overline{h}_1[k]$ and $\overline{h}_2[k]$ set to one, all training symbols $+1$).

As can be seen, $L_{\mathrm{T}} > 60$ training symbols are required in the case $E_s/N_0 \to \infty$, in order to estimate both frequency offsets with an error of 3% or better (dotted lines). In the case of finite E_s/N_0, the required number of training symbols might be greater, depending on the current realizations of the noise samples.

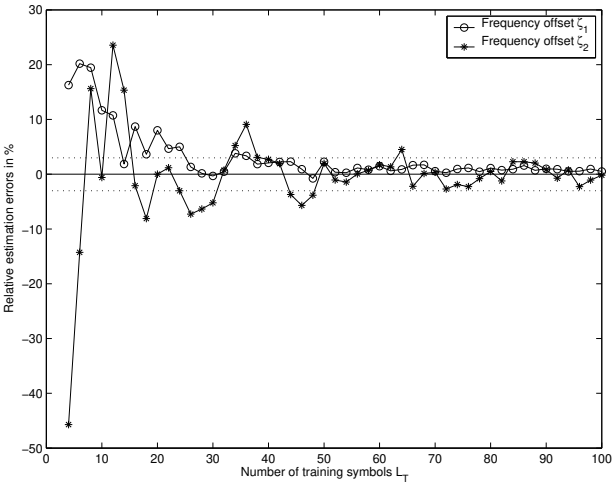

Fig. 7. Example for the relative estimation errors as a function of the number of training symbols, L_{T}, given $E_s/N_0 = 20$ dB.

B. Blind Estimation Method

In the case of QPSK symbols $x[k] \in \{+1, +\mathrm{j}, -1, -\mathrm{j}\}$, a common blind frequency-offset estimation method is to raise the received symbols $y[k]$ to the power of four and subsequently perform a fast Fourier transform (FFT) [19, Ch. 6.3.1]. Given a (1x1)-system, $y^4[k]$ yields

$$\begin{aligned} y^4[k] \;&\doteq\; \left(\overline{h}[k]\,x[k] \,+\, n[k]\right)^4 \\ &=\; \overline{h}^4[k]\,x^4[k] \,+\, \eta[k], \end{aligned} \tag{23}$$

where $\eta[k]$ consists of five additive terms that are regarded as noise in the following. Irrespective of the current realization of $x[k]$, the desired term $\overline{h}^4[k]\,x^4[k]$ results as

$$\overline{h}^4[k]\,x^4[k] \;=\; \left(h\,\mathrm{e}^{\mathrm{j}2\pi\zeta k}\right)^4 x^4[k] \;=\; h^4\,\mathrm{e}^{\mathrm{j}2\pi\,4\zeta\,k}\,. \tag{24}$$

Therefore, an FFT of the sequence $\{y^4[k]\}_{k=0,\ldots,L_{\mathrm{B}}-1}$ will yield a spectral line at 4ζ plus noise. If the noise power is suf-

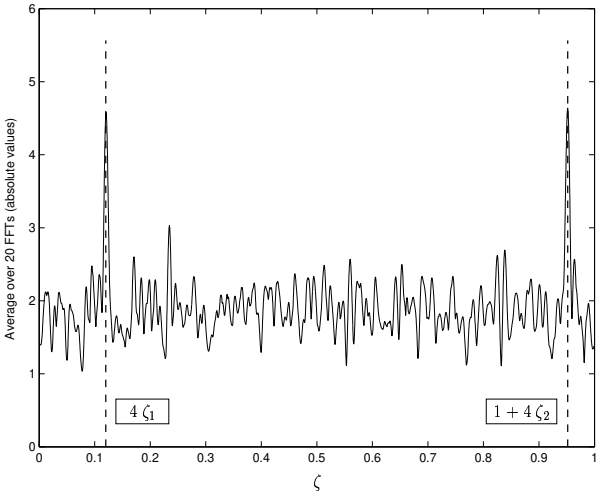

Fig. 8. Blind frequency-offset estimation method for the Alamouti scheme: Absolute FFT values obtained by averaging over 20 data blocks, clearly showing the spectral lines that are due to the frequency offsets ζ_1 and ζ_2.

ficiently small, the spectral line may be detected by means of a simple maximum search over the absolute values of the FFT output.

The same strategy may, in principle, as well be pursued in the case of the distributed Alamouti scheme. One obtains

$$y^4[k] \;=\; c^4\,h_1^4\,\mathrm{e}^{\mathrm{j}2\pi\,4\zeta_1\,k} \;+\; c^4\,h_2^4\,\mathrm{e}^{\mathrm{j}2\pi\,4\zeta_2\,k} \;+\; \tilde{\eta}[k]\,, \qquad (25)$$

where $\tilde{\eta}[k]$ consists of altogether 20 additive noise terms.

Simulations conducted for a quasi-static Rician fading channel with Rice factor $K = 0$ dB and $E_s/N_0 = 20$ dB have shown that in the case of the (1x1)-system, detection of the frequency offset ζ is typically possible on basis of just a single data block. Generally, the resulting FFT values should be averaged over few data blocks, in order to reduce the influence of the noise and thus to guarantee reliable detection. As opposed to this, in the case of the Alamouti scheme one needs to average over a comparably large number of data blocks, so as to enable a reliable detection of the frequency offsets ζ_1 and ζ_2.

Fig. 8 illustrates the above blind estimation method for the Alamouti scheme. As an example, absolute FFT values are shown that were obtained by averaging over 20 data blocks ($K = 0$ dB, $E_s/N_0 = 20$ dB). The block length was chosen as $L_{\mathrm{B}} = 128$ and the length of the FFT was 4096. As earlier, the frequency offsets were set to $\zeta_1 = +0.03$ and $\zeta_2 = -0.012$ (the chosen FFT length enables distinction of two points that differ by 0.5% of ζ_2). As can be seen, the spectral lines at $4\zeta_1$ and $1+4\zeta_2$ (due to the negative sign of ζ_2) are clearly visible and may be detected by means of a simple maximum search.

V. Conclusions

In this paper, it has been shown that the performance of a distributed Alamouti scheme in a simulcast network can be significantly degraded by frequency offsets that may occur at the individual transmitting nodes. Different receiver concepts have been considered, and their sensitivity to the quality of the frequency-offset estimates has been illustrated. It turned out that the frequency-offset estimates are required to be quite accurate, in order to keep the resulting orthogonality loss small and thus the occurring performance loss. Finally, two different methods have been discussed to estimate the frequency offsets. It has been demonstrated, that frequency-offset estimation is more difficult than in the case when there is only a single transmitting node.

Acknowledgment

The authors would like to thank Ralf Seeger, Ronald Böhnke, Dirk Wübben, Jürgen Rinas, Dr. Volker Kühn (Department of Communications Engineering, University of Bremen), and Dr. Jörg Kliewer (Institute for Circuits and System Theory, University of Kiel) for fruitful discussions and helpful suggestions.

References

[1] D. Gesbert, M. Shafi , D. Shiu, P. J. Smith, and A. Naguib, "From theory to practice: An overview of MIMO space-time coded wireless systems," *IEEE J. Select. Areas Commun.*, vol. 21, no. 3, pp. 281-302, Apr. 2003.

[2] V. Tarokh, N. Seshadri, and A. R. Calderbank, "Space-time codes for high data rate wireless communication: Performance criterion and code construction," *IEEE Trans. Inform. Theory*, vol. 44, no. 2, pp. 744-765, Mar. 1998.

[3] V. Tarokh, A. Naguib, N. Seshadri, and A. R. Calderbank, "Space-time codes for high data rate wireless communication: Performance criteria in the presence of channel estimation errors, mobility, and multiple paths," *IEEE Trans. Commun.*, vol. 47, no. 2, pp. 199-207, Feb. 1999.

[4] V. Tarokh, H. Jafarkhani, and A. R. Calderbank, "Space-time block coding for wireless communications: Performance results," *IEEE J. Select. Areas Commun.*, vol. 17, no. 3, pp. 451-460, Mar. 1999.

[5] V. Tarokh, H. Jafarkhani, and A. R. Calderbank, "Space-time block codes from orthogonal designs," *IEEE Trans. Inform. Theory*, vol. 45, no. 5, pp. 1456-1467, June 1999.

[6] A. Wittneben, "Basestation modulation diversity for digital SIMULCAST," in *Proc. IEEE Veh. Technol. Conf. (VTC'91)*, 1991, pp. 848-853.

[7] D. Kim, G. L. St¨uber, and N. Hightower, "Performance of simulcast systems in mobile radio environments," in *Proc. IEEE Veh. Technol. Conf. (VTC'97)*, 1997, pp. 495-499.

[8] A. Sendonaris, E. Erkip, and B. Aazhang, "User cooperation diversity – Part I and II," *IEEE Trans. Commun.*, vol. 51, no. 11, pp. 1927-1948, Nov. 2003.

[9] J. N. Laneman and G. W. Wornell, "Distributed space-time-coded protocols for exploiting cooperative diversity in wireless networks," *IEEE Trans. Inform. Theory*, vol. 49, no. 10, pp. 2415-2425, Oct. 2003.

[10] P. A. Anghel, G. Leus, and M. Kaveh, "Distributed space-time coding in cooperative networks," in *Proc. V IEEE Nordic Signal Processing Symposium (NORSIG–2002)*, 2002, paper no. SunAmOR2–2.

[11] S. M. Alamouti, "A simple transmit diversity technique for wireless communications," *IEEE J. Select. Areas Commun.*, vol. 16, no. 8, pp. 1451-1458, Oct. 1998.

[12] J. Mietzner, M. Kautza, and P. A. Hoeher, "Application of the Alamouti scheme in resilient microwave radio links," *IEE Electron. Lett.*, vol. 39, no. 12, pp. 927-928, June 2003.

[13] J. Mietzner, J. Eick, and P. A. Hoeher, "Frequency-offset sensitivity of resilient microwave links applying the Alamouti scheme," in *Proc. 5th Int. ITG Conf. on Source and Channel Coding (SCC)*, 2004, pp. 165-172.

[14] X.-B. Liang and X.-G. Xia, "On the nonexistence of rate-one generalized complex orthogonal designs," *IEEE Trans. Inform. Theory*, vol. 49, no. 11, pp. 2984-2989, Nov. 2003.

[15] Z. Chen, J. Yuan, B. Vucetic, and Z. Zhou, "Performance of Alamouti scheme with transmit antenna selection," *IEE Electron. Lett.*, vol. 39, no. 23, pp. 1666-1668, Nov. 2003.

[16] G. Bauch, *"Turbo-Entzerrung" und Sendeantennen-Diversity mit "Space-Time-Codes" im Mobilfunk.* PhD thesis, Department of Communications Engineering, Munich University of Technology, 2001. (in German).

[17] E. Biglieri, G. Taricco, and A. Tulino, , "Performance of space-time codes for a large number of antennas," *IEEE Trans. Inform. Theory*, vol. 48, no. 7, pp. 1794-1803, Jul. 2002.

[18] J. G. Proakis, *Digital Communications.* 4th ed., New York: McGraw-Hill, 2001.

[19] R. D. Gitlin, J. F. Hayes, and S.B. Weinstein, *Data Communications Principles.* New York: Plenum Press, 1992.